PCCP

View Online / Journal Homepage
Dynamic Article Links

Cite this: DOI: 10.1039/c2cp40695k

www.rsc.org/pccp

PAPER

Charge regulation in redox active monolayers embedded in proton exchanger surfaces

A. M. Ricci,[a] M. Tagliazucchi[b] and E. J. Calvo*[c]

Received 5th March 2012, Accepted 8th May 2012
DOI: 10.1039/c2cp40695k

Experimental evidence of the variation in redox potential of osmium pyridine complexes tethered to a Au surface by thiol or diazonium chemistry at different ionic concentration and electrolyte pH is described. The interplay between the charged redox and acid groups is described by a charge regulation model based on PM-IRRAS spectroscopic evidence on the different degrees of surface protonation.

Introduction

Organized self-assembled monolayers have emerged as attractive model systems for studying the chemistry of organic surfaces.[1–3] Self-assembled monolayers (SAMs) formed on Au using thiol compounds with acidic functionalities exposed to solution have found utility in numerous areas since they are good model systems for the study of proton transfer reactions[4,5] which are, in turn, relevant to many fields such as surface wetting,[6] adhesion,[7–9] colloid, foam and emulsion stability[10] and the biophysical stability of membranes, proteins and other biological super-structures.[11] Further uses to which such monolayer-coated surfaces have been applied include lithography[12,13] and electron transfer studies.[14–18] Moreover, carboxylic acid groups are especially useful in cases where further reaction with the surface is desired such as protein immobilization at well-defined distances.[19,20] An important aspect of controlling these interactions is knowledge of the difference between the solution property values of the surface modifiers, such as pK_a, and their related properties once confined to the surface, such as $pK^{1/2}$ or apparent surface pK_a. Several studies have probed the acidity of ω-mercaptocarboxylic acid SAMs on gold using a variety of techniques, including capacitance,[21] piezoelectric quartz crystal microbalance,[22,23] spectroscopic,[24] electrochemical[25,26] and contact angle methods.[10,27,28]

A widespread method for post-functionalizing self-assembled monolayers uses amide-bond formation between a carboxylic end-group on the thiol and an amine at the end of the molecule to be grafted (or *vice versa*). Complete functionalization is almost never achieved and therefore the local environment of SAM-attached molecules is rich in acid–base functionalities. Local electrostatics play a key role in regulating chemical/biochemical activity and therefore it is important to address how the electrostatic environment is created from the coupling between the acid–base equilibrium of these groups, the electrode potential and the ion distribution.

The electrostatic interactions at self-assembled molecular films of charged thiols on gold have been described by Molinero and Calvo.[29] Smith and White developed a theory of the interfacial potential distribution and reversible voltammetric response of electrodes coated with electroactive molecular films[30] and the voltammetry response of molecular films containing acid–base groups.[31]

In this paper we describe a systematic study of the effect of electrolyte ionic concentration and pH on the redox behaviour of osmium groups tethered to a Au electrode by thiol and diazonium chemistry. The results are quantitatively explained in terms of charge regulation at the surface resulting from the interplay of redox and carboxylate groups.[32]

A qualitative report on the coupling of acid-base and redox functions in mixed functional thiols on Au has been disclosed by Reinhoudt and co-workers.[33] Theoretical models quantitatively describing the effect of acid–base groups on the redox equilibrium of neighboring species have been addressed for polymer films,[32] but not for quasi-two-dimensional SAMs.

Experimental

Chemicals

The following chemicals were used as received: 16-mercaptohexadecanoic acid (Sigma-Aldrich), 11-mercaptoundecanoic acid (Sigma-Aldrich), 4-mercaptobenzoic acid (Sigma-Aldrich), 1-ethyl-3-(3-dimethylamino-propyl)-carbodiimide (Aldrich), *N*-hydroxysuccinimide (Aldrich), 4-2-hydroxyethyl-1-piperazine-ethanesulfonic acid (HEPES) (Sigma-Aldrich), potassium nitrate (Merck), tetrabutylammonium tetrafluoroborate (Fluka), 4-aminobenzoic acid (Sigma-Aldrich), iso-amyl nitrite (Sigma-Aldrich), sodium fluoroborate (Sigma-Aldrich), acetonitrile (Sintorgan, Buenos Aires, Argentina), tetrafluoroboric acid

[a] *Chemistry Department, Northwestern University, 2145 Sheridan Road, Evanston, IL 60208-3113, USA. E-mail: aricci@aluar.com.ar*
[b] *ALUAR S.A. Aluminio Argentino, Puerto Madryn, Chubut, Argentina. E-mail: m-tagliazucchi@northwestern.edu*
[c] *INQUIMAE-DQIAyQF, Facultad de Ciencias Exactas y Naturales, UBA Pabellon 2, Ciudad Universitaria, Buenos Aires, Argentina. E-mail: calvo@qi.fcen.uba.ar*

(50% solution, Riedel de Haën), ethyl ether (Sintorgan), ethanol (Sintorgan, Buenos Aires, Argentina), sodium nitrate (Biopack).

Preparation of gold surfaces

Silicon(100) wafer substrates were coated with a 20 nm titanium and 20 nm palladium adhesion layer and a 200 nm gold layer, thermally evaporated with an Edwards Auto 306 vacuum coating system at $P < 10^{-8}$ bar, and employed as electrodes. Before surface modification, the electrode potential was cycled in 2 M sulfuric acid between 0 and 1.6 V at 0.1 V s^{-1} to check for surface contamination, and electrochemically active areas were calculated from the reduction peak of gold oxide. The surface roughness was 1.5–2. A glass electrochemical cell with a Pt counter electrode and an Ag/AgCl, 3 M KCl reference electrode was employed, and potentials herein are reported with respect to this reference.

Thiol monolayers on gold substrates were obtained by overnight immersion of the electrodes in 1 mM ethanolic solutions of the corresponding thiol. The benzoic acid was grafted onto the electrode surface by electrochemical reduction of the corresponding diazonium salt using chronoamperometry (0.4 V, 5 min in 5 mM 4-carboxybenzenediazonium tetrafluoroborate/0.1 M tetrabutylammonium tetrafluoroborate/acetonitrile).

The monolayers were post-functionalized with the $[Os(bpy)_2Cl(py–CH_2–NH_2)]PF_6$ complex. After the initial derivatization, the gold surfaces were incubated in 40 mM 1-ethyl-3-(3-dimethylamino-propyl)-carbodiimide (EDC)/10 mM *N*-hydroxy succinimide (NHS) solution for 1 h, and dipped in 0.25 mM $[Os(bpy)_2Cl(py–CH_2–NH_2)]PF_6$/0.05 M HEPES buffer (*N*-2-hydroxy-ethyl-piperazine-*N*′-2-ethane-sulfonic acid) pH 7.3, $I = 0.1$ M KNO_3 for 12 h. The synthesis of the osmium complex and the diazonium salt has been described elsewhere.[34]

IR experiment

Polarization modulation infrared reflection absorption spectroscopy (PM-IRRAS) experiment was performed on a Thermo Nicolet 8700 (Nicolet, Madison, WI) spectrometer equipped with a custom-made external tabletop optical mount, a MCT-A detector (Nicolet), a photoelastic modulator, PEM (PM-90 with II/Zs50 ZnSe 50 kHz optical head, Hinds Instrument, Hillsboro, OR), and a synchronous sampling demodulator, SSD (GWC Instruments, Madison, WI). The IR spectra were acquired with the PEM set for a half wave retardation at 1450 cm^{-1} for the CH bending and aromatic region and for stretching modes associated with the COOH group. The angle of incidence was set at 80°, which gives the maximum of mean square electric field strength for the air–gold interface. The demodulation technique developed by Corn *et al.*[35,36] was used in this work. The signal was corrected by the PEM response using a method described by Frey *et al.*[37] Typically 1000 scans were performed and the resolution was set to 4 cm^{-1}.

Electrochemical experiment

Electrochemical measurements were carried out with an Autolab V 30 system (Eco Chemie, Utrecht, the Netherlands) controlled by the General Purpose Electrochemical Software (GPES). This potentiostat is equipped with a 750 kHz bandwidth ADC750 fast sampling module and a scangen analog sweep module. All experiments were carried out at room temperature (20 ± 2 °C). Cyclic voltammetry experiments were performed in a purpose-built, three-electrode Teflon cell, with an electrode exposed area of approximately 0.28 cm^2 delimited by an inert "o" ring.

Results

The systems analyzed herein consist of monolayers of carboxylic-acid terminated molecules formed by either self-assembled mercaptocarboxylic acids or by electroreduction of diazonium salts and subsequent post-functionalization with a redox osmium complex: $[Os(bpy)_2Cl(py–CH_2–NH_2)]PF_6$ (Scheme 1). Since the size of the underlying molecules is much smaller than that of the osmium complex, the post-functionalization efficiency is always less than 100%. We have estimated the efficiency from the thiol coverage (MUA or SPhCOOH) and the electroactive charge of the osmium complex by assessing the thiol coverage from desorption reduction charge and the charge under the anodic and cathodic peaks in the Os(II/III) cyclic voltammogram, respectively.

From this estimation, the post-functionalization efficiency for Au–MUA–Os results in ≈20% and for Au–SPhCOOH–Os ≈3%. Considering that the post-functionalization reaction is a nucleophilic acyl substitution, the low efficiency observed in the second system can be attributed to the deactivation of the carboxylic group by the thiol group at the *para* position of the aromatic ring.

The degree of reaction of surface carboxylates with amines in the osmium complex determines the ratio of redox to carboxylate groups on the electrode surfaces which results in a large fraction of surface unsubstituted carboxylic groups, whose ionization state depends on the solution pH. Thus the solution pH determines the surface charge which can strongly affect the redox chemistry of these electrodes.

The surface voltammetric waves of the modified electrodes shift with electrolyte pH as shown in Fig. 1 for solutions of pH 3, 5 and 11 respectively. The cyclic voltammetry curves are similar in terms of peak width at half maximum, charge and peak current. Similar shifts have been previously observed for SAMs containing pH-responsive redox couples.[38] However, the redox potential of the osmium complex used in this work and measured in solution is pH-independent. Therefore we ascribe the shift of its formal potential in the SAM to its intermolecular interactions with neighboring pH-dependent carboxylates. The formal potential varies significantly with pH as can be appreciated

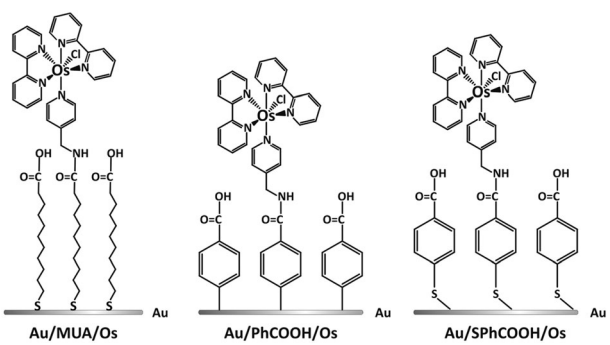

Scheme 1 Surface molecular structures.

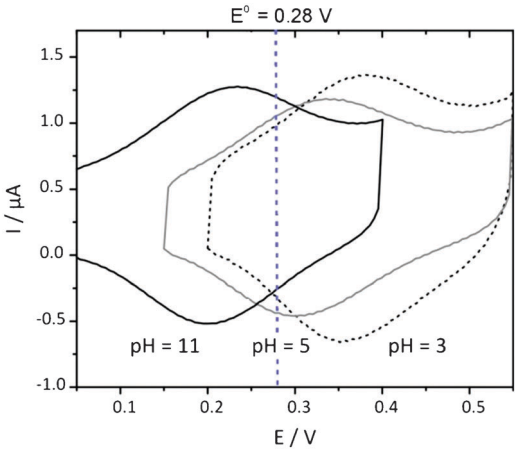

Fig. 1 Cyclic voltammetry of Au–MUA–Os in 4 mM $NaNO_3$ solutions of pH 11, 5 and 3. The pH was adjusted by adding 1 mM HNO_3 and 1 mM NaOH respectively. The dashed vertical line indicates the redox potential of the Os(II/III) complex in solution.

when comparing with the formal redox potential of the soluble redox couple ($[Os(2,2'\text{-bpy})_2Cl(pyCHO)]^{+/2+}$), *ca.* 0.28 V *vs.* Ag/AgCl (0.24 V *vs.* SCE[39]) as shown by a dashed line in Fig. 1. At pH = 3 the formal potential shifts towards more positive values whereas at pH = 11, a negative shift is observed.

The state of ionization of the carboxylic groups at the surface for different solution pH has been investigated using polarization modulation infrared reflection absorption spectroscopy (PM-IRRAS). Fig. 2 depicts PM-IRRA spectra of a Au surface modified with a monolayer of MUA, and the same surface exposed, respectively, to acid and alkaline solutions. Two infrared spectra were obtained for a Au substrate modified with a monolayer of MUA after immersion in 1 mM NaOH and in 1 mM HNO_3 solutions for 15 minutes, respectively. In both cases the PEM was set at λ_o = 1450 cm^{-1}. The initial spectrum shows bands at 1726 cm^{-1}, 1540 cm^{-1} and 1440 cm^{-1} characteristic of a mixture of protonated and deprotonated carboxylate groups at the surface.

After the immersion of the sample in a solution of pH 11 two bands (1540 and 1488 cm^{-1}) can be observed in the infrared

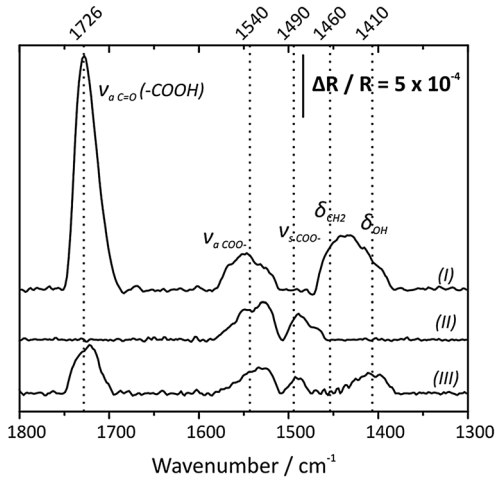

Fig. 2 PM-IRRAS spectra of a gold surface (I) modified with MUA and (II) after immersion in 1 mM NaOH and (III) in 1 mM HNO_3 solutions, respectively.

spectrum which are associated with the antisymmetric and symmetric stretching modes of the carboxylate group (ν_{aCOO-} and ν_{sCOO-}), respectively, and simultaneous disappearance of the 1726 cm^{-1} mode. On the other hand, after immersion in a solution of pH 3, two new bands appear at 1722 and 1409 cm^{-1}. These infrared bands can be related to the presence of protonated carboxylic acid groups on the surface, since they can be assigned to the antisymmetric stretching mode of the carbonyl group ($\nu_{aC=O}$) and the deformation mode of the hydroxyl group (δ_{OH}) characteristic of this functional group. These experimental spectroscopic evidences confirm that the monolayer effectively changes its protonation state, and thus its surface charge, with electrolyte solution pH. It is worthwhile to mention that under the conditions of this experiment, PM-IRRAS provides qualitative information about the presence or absence of functional groups within the monolayer, but we believe that the relative intensities of the bands cannot be used for quantification. Therefore, further analysis of the surface populations based on PM-IRRAS was not attempted.

In order to further analyze the effect of surface protonation on the electrochemical response of an intrinsically pH-independent redox couple, we studied three molecular systems at the Au surface at different pH: Au–MUA–Os, Au–SPhCOOH–Os and Au–PhCOOH–Os. Cyclic voltammetry was recorded for these surfaces in electrolyte solutions of different pH from 3 to 11 prepared employing mixtures of $NaNO_3$–1 mM HNO_3 and $NaNO_3$–1 mM NaOH solutions, where the $NaNO_3$ concentration was either 4 mM or 0.1 M.

Fig. 3 shows the variation of the formal potential with pH when the ionic strength of the solutions was set to 4 mM and 0.1 M, respectively. A clear decrease in the redox potential with increasing electrolyte pH is observed for the three systems; the effect is stronger at low ionic strength. To analyze these results, we have extended the model developed by Smith and White,[30,31] in order to consider the coupling that exists between the acid–base and redox equilibria within the film (see details in the Appendix). There is no explicit solution for the pH-dependence of the peak position, but we found analytical expressions that are parametric in f (the dissociation fraction of the carboxylates):

$$E^{peak}(f) = E^0 + \frac{2RT}{F}\operatorname{asinh}\left[\frac{-\Gamma_{HA/A}f + \Gamma_{Os}\frac{(Z_{Os(III)}+Z_{Os(II)})}{2} + \frac{(E^0-E_{pzc})C_{film}}{F}}{\left(\frac{8C_{salt}\varepsilon_s\varepsilon_0 RT}{F^2}\right)^{1/2}}\right] \quad (1a)$$

$$pH(f) = pK_a - \frac{2}{2.303}\operatorname{asinh}\left[\frac{-\Gamma_{HA/A}f + \Gamma_{Os}\frac{(Z_{Os(III)}+Z_{Os(II)})}{2} + \frac{C_{film}(E^0-E_{pzc})}{F}}{\left(\frac{8C_{salt}\varepsilon_s\varepsilon_0 RT}{F^2}\right)^{1/2}}\right] + \log\left(\frac{f}{1-f}\right) \quad \text{for } 0 < f < 1. \quad (1b)$$

where E^0 is the standard potential of the redox couple, E_{pzc} is the zero charge potential of the metal electrode, $\Gamma_{HA/A}$ and Γ_{Os} are the surface coverages of acid–base sites (unreacted thiols)

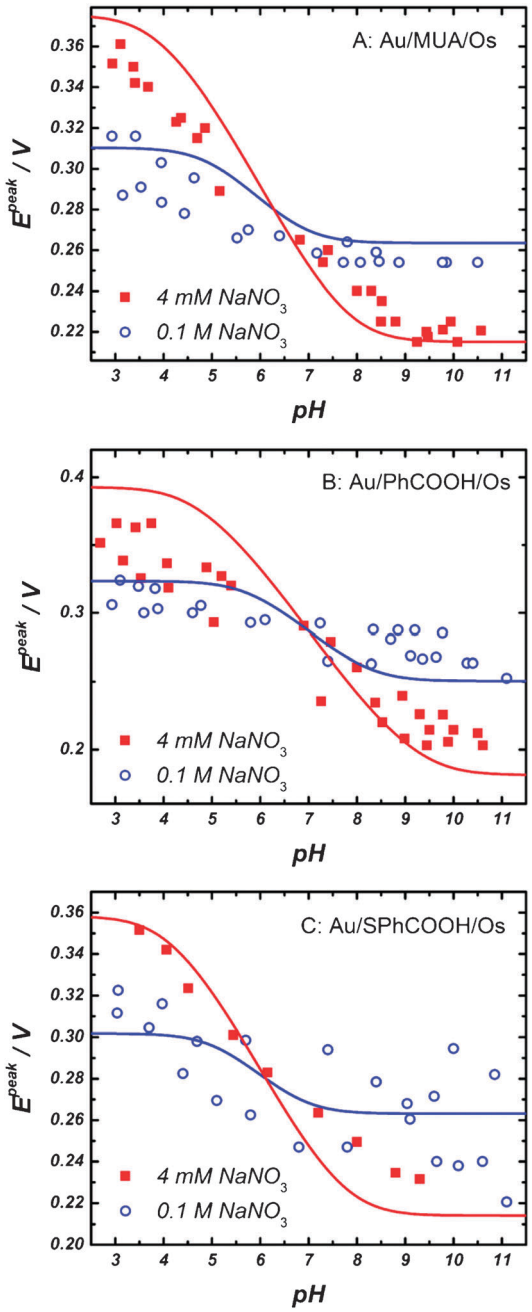

Fig. 3 Formal potential of the Os(II/III) redox couple (determined from the peak potential in the cyclic voltammogram) as a function of solution pH at constant ionic strength for (A) Au–MUA–Os; (B) Au–PhCOOH–Os; and (C) Au–SPhCOOH–Os.

and electroactive molecules (osmium complexes), respectively, z_O and z_R are the charges associated with the oxidized and reduced species, C_{film} is the film capacitance and ε_o is the vacuum permittivity and ε_s the relative dielectric constant of the organic film while C_{salt} is the concentration of the electrolyte. The fitting parameters of the model are: standard potential (E^0), the constant for acid–base equilibrium (pK_a, this corresponds to the value in solution, *i.e.* in the absence of an electrostatic surface potential) and the surface coverage of the underlying layer (either formed by thiols or from reduction of the diazonium salt) and the osmium complex.

Table 1 Best fit parameters to eqn (1) and (2) with data in Fig. 3 and 4

	E^0/V	pK_a	Γ_{Os}/ pmol cm^{-2}	$\Gamma_{HA/A}$/ pmol cm^{-2}	$(E^0 - E_{pzc})$ C_F/μC cm^{-2}
Au–MUA–Os	0.282	6.0	10	37	0.9
Au–SPhCOOH–Os	0.280	6.0	8.0	30	0.5
Au–PhCOOH–Os	0.287	7.0	10	60	1.5

The best fit using eqn (1) is indicated by solid lines in Fig. 3 and Table 1 summarizes the parameters obtained for each system.

To explain the behavior observed in Fig. 3 it is worthwhile remembering that a negative (positive) electrostatic environment will increase (decrease) the free energy cost of transferring an electron to the osmium complex and thus it will decrease (increase) its apparent redox potential. The local electrostatic potential is controlled by the total electrostatic charge in the film, which has contributions from the negative deprotonated carboxylates and the positive osmium complexes. Therefore the balance between positive and negative charges in the SAM controls the observed pH–potential dependence and gives rise to three well-defined regions which we shall refer as (I), (II) and (III). Region (I) includes the range of pH < 3, where the charge density in the film does not change because at this pH practically all the –COOH groups are protonated. In this case, the charge on the surface is given only by the redox centers. The second region comprises the interval of pH between 3 and 8, and it shows the greatest variation of formal potential with pH. This behavior can be associated with the deprotonation of acidic groups with increasing solution pH. Finally, region (III) corresponds to pH > 8, where the potential remains almost constant because in this pH interval the acid groups are almost completely deprotonated. In this region, E^{peak} is below the formal potential observed for the soluble analogs because the surface charge is positive due to the charge of the osmium complex (which is $+1/+2$ for a reduced/oxidized osmium site).

The influence of the ionic strength on the formal potential of the tethered redox complex has been examined by a similar experiment keeping the pH constant at 3 and 11, respectively, and varying the concentration of the supporting electrolyte between 4 mM and 2 M. Each set of data was again analyzed on the basis of the modified Smith–White model using eqn (2), which is derived in the Appendix. This equation describes implicitly (using a parametrization in f) the dependence of the formal potential of the osmium couple with the ionic strength of the adjacent solution.

$$E^{peak}(f) = E^0 + \frac{2.303RT}{F}\left[pK_a - pH + \log\left(\frac{f}{1-f}\right)\right] \quad (2a)$$

$$C_{salt}(f) = \frac{F^2}{8\varepsilon_s\varepsilon_0 RT} \times \left[\frac{-\Gamma_{HA/A} f + \Gamma_{Os}\frac{(Z_{Os(III)}+Z_{Os(II)})}{2} + \frac{(E^0-E_{pzc})C_{film}}{F}}{\sinh\left(\frac{2.303}{2}\left(pK_a - pH + \log\left(\frac{f}{1-f}\right)\right)\right)}\right]^2 \quad \text{for } 0 < f < 1 \quad (2b)$$

Fig. 4 shows the results obtained for the three systems studied: Au–MUA–Os, Au–SPhCOOH–Os and Au–PhCOOH–Os.

The line in Fig. 4 is the best fit of the experimental data to eqn (2). It should be stressed that we simultaneously fit the experiments as a function of salt concentration and pH (Fig. 3 and 4) to eqn (1) and (2) for each experimental system (*i.e.* each different grafted thiol or diazonium salt). This procedure yields the parameters with the best fit to both sets of experimental data for each system. This is very important because the data obtained in both experiments have been described with the same model. Therefore, the parameters shown in Table 1 are the same as that used in eqn (2).

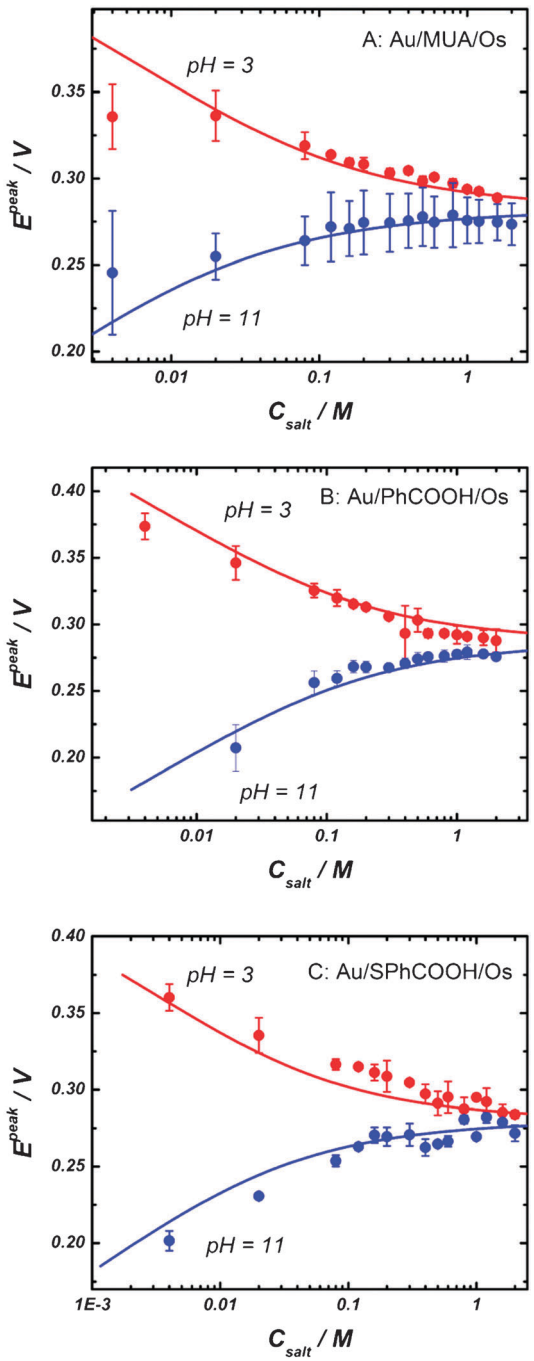

Fig. 4 Formal potential variation with ionic strength at fixed pH for (A) Au–MUA–Os; (B) Au–PhCOOH–Os; and (C) Au–SPhCOOH–Os.

In all cases, a greater variation of E^{peak} is observed for the lower $NaNO_3$ concentration employed. This effect arises from the screening of electrostatic interactions in the SAM due to the mobile ions in solution. In other words, the absolute value of the local electrostatic potential sensed by a redox group in the film decreases with increasing ionic strength, regardless of the sign of the surface charge. Hence, the lower the concentration of a supporting electrolyte the greater is the contribution and impact of pH on the formal potential.

In Fig. 4 a shift of E^{peak} is evident when the concentration of the supporting electrolyte decreases. At pH = 3, this displacement is positive, while at pH = 11, it is negative. This arises from the same surface charge phenomenon as the dependence of E^{peak} with pH. In this case, at a given solution pH the higher the supporting electrolyte concentration, the larger the screening of the electrostatic interactions of surface confined redox species due to screening of the charge density at the electron transfer plane that attenuates the potential difference between this plane (φ^{PET}) and the bulk solution (φ^{S}).

For all these reasons, increasing the ionic strength of the solution reduces the formal potential shift towards the value observed for the free redox couple in solution, *i.e.* 0.28 V. The slopes of the curves indicate that the charge compensation is satisfied with the adsorption of anions when the surface excess is positive and cation adsorption, when this excess is negative. The phenomenon of surface potential is analogous to Donnan or membrane potential in films thicker than the Debye length.[40,41]

The standard potential obtained from the best fit of the experimental data to the equations derived with the Smith–White model is in good agreement with that reported for the same Os(II/III) complex in solution (0.28 V).[39]

The pK_a retrieved from the theory corresponds to the pK_a of the acid–base group in the absence of the surface electrostatic potential. In other words, they do not correspond to the apparent pK_a on the surface that it is experimentally determined as the pH of the solution for which half of the groups on the surface are ionized (p$K^{1/2}$).[10,27,28] Interestingly, the pK_a values reported in Table 1 are larger than those measured for the isolated molecules in solution (pK_a^{bulk} = 4.8 for MUA[42]). Therefore, factors beyond the surface potential (and thus not included in our model) may significantly contribute to the free energy of protonation; such factors may include: Born energy, discreetness of charge[43] and ion correlations.

The redox surface coverages obtained from our analysis can be compared with those measured by electrochemical charge integration for each system: 40 pmol cm^{-2} for Au–MUA–Os, 7 pmol cm^{-2} for Au–SPhCOOH–Os and 104 pmol cm^{-2} for Au–PhCOOH–Os. The osmium-complex surface coverages obtained from the fitting are therefore of the same order of magnitude as those derived from the integrated redox charge, although it is slightly lower than that expected for Au–PhCOOH–Os.

The surface coverages for the carboxylic/carboxylate groups were estimated by reductive desorption in the case of the thiols. These were 1.1 and 0.9 nmol cm^{-2} for MUA and SPhCOOH, respectively (these values are in good agreement with those expected for the compact thiol monolayers[44,45]). These values are, however, 30 times larger than those estimated using our model (see Table 1). AFM experiments by the Bard

group have shown similar discrepancies. In these experiments, the real surface charge of bare gold electrodes[46] or redox-active monolayers[47] was found to be 10 to 30 times larger than that derived from the surface potential (measured by AFM force measurements).

Conclusions

In this work, we studied the redox formal potential of the pH independent Os(II/III) redox couple obtained by cyclic voltammetry in solutions of different pH and salt concentration. We show that the formal potential of the redox couple is determined by the protonation equilibrium of carboxylate species at the surface and shielding of electrostatic interactions of surface charge at high ionic concentration. The redox group in this work acts therefore as a redox reporter to determine the electrostatic potential of the surface.

We presented a modified Smith–White model to analyse the experimental data. This model includes a description of the electrostatic potential at the metal–SAM–electrolyte interface coupled to the acid–base and redox equilibria. The model can be solved analytically as a function of the parameter f (the dissociation fraction of the acid–base species) and produces good quality fittings to the experimental data. However, the calculated surface coverage of the thiols is much smaller than those determined by reductive desorption.

Interestingly, discrepancies between real and effective surface charges were previously reported for AFM force measurements,[46] which, alike our method, determine the total surface charge from a surface potential measurement by using the Poisson–Boltzmann equation (*i.e.* the Gouy–Chapman model, which is also used in our model). This observation suggests that the underestimation of the density of surface-confined charged molecules can be traced back to the use of the mean-field Poisson–Boltzmann equation. An important conclusion from the present work is that this difference does not arise from charge regulation due to the protonation of the weakly acid monolayer because (i) we explicitly include charge regulation due to acid–base equilibrium in our analysis and (ii) lower-than-expected surface coverages for thiols are also retrieved from the data at pH 11, however COOH was not detected in the PM-IRRA spectrum for this pH.

The formation of ion pairs between cations in solution (Na^+) and carboxylates on the surface and ion–ion correlations are possible causes for the disagreement in the thiol surface coverages. Further theoretical work analysing the interplay between electrostatic and non-electrostatic interactions and charge regulation beyond the Poisson–Boltzmann model is thus necessary to reconcile the real surface coverages with those determined from surface potential measurements.

Appendix

This appendix presents an extension of the Smith and White model[30,31] to consider a film bearing both redox and acid–base groups. The electrochemical potential of the species i in each phase j where it is present can be expressed as:

$$\mu_i = \mu_i^0 + RT\ln(a_i^j) + z_iF\phi_i^j, \qquad \text{(A1)}$$

where a_i^j is the activity of ion i in phase j, ϕ_j is the potential of phase j, F is the Faraday constant and z_i and μ_i^o are the charge and the standard chemical potential of the species i, respectively.

For the acid–base equilibrium at the plane of acid dissociation (PAD):

$$HA(PAD) \overset{K_a}{\rightleftharpoons} H^+(PAD) + A^-(PAD) \qquad \text{(A2)}$$

we can write,

$$\begin{aligned}\mu_{H^+} &= \mu_{H^+}^0 + RT\ln[H^+]^s + F\varphi^s \\ &= \mu_{H^+}^0 + RT\ln[H^+]^{PDA} + F\varphi^{PDA} \\ \mu_{A^-} &= \mu_{A^-}^0 + RT\ln[A^-]^{PDA} - F\varphi^{PDA} \\ \mu_{HA} &= \mu_{HA}^0 + RT\ln[HA]^{PDA}\end{aligned} \qquad \text{(A3)}$$

Substituting eqn (A3) into the following equilibrium condition:

$$\mu_{HA} = \mu_{H^+} + \mu_{A^-} \qquad \text{(A4)}$$

yields upon rearrangement,

$$\Delta\varphi^{PDA-S} = \varphi^{PDA} - \varphi^s = \frac{2.303RT}{F}\left[pK_a - pH + \log\left[\frac{f}{1-f}\right]\right] \qquad \text{(A5)}$$

where f is the degree of acid deprotonation, given by:

$$f = \frac{[A^-]^{PAD}}{[A^-]^{PAD} + [HA]^{PAD}} \qquad \text{(A6)}$$

Eqn (A6) relates the potential difference between the PAD and the electrolyte solution with the degree of protonation of the weak acid at the surface.

The overall electrochemical reaction in the system is the combination of the half reactions occurring at the plane of electron transfer (PET) and the reference electrode,

$$Os(III)^{(PET)} + Ag(Ag) + Cl^-(s) \rightleftharpoons Os(II)^{(PET)} + AgCl(AgCl) \qquad \text{(A7)}$$

and thus in equilibrium we can write,

$$\mu_{Os(III)} + \mu_{Ag} + \mu_{Cl^-} = \mu_{Os(II)} + \mu_{AgCl} \qquad \text{(A8)}$$

Substituting the electrochemical potential of each of the species into eqn (A8) by their definition according to eqn (A1) and using $E = (\phi^M - \phi^{Ag})$, $a_{Ag}^{Ag} = a_{AgCl}^{AgCl} = 1$ and $a_{Cl^-} = 3$ M[31] yields:

$$E = E^0 + \frac{RT}{F}\ln\left(\frac{a_{Os(III)}^{PET}}{a_{Os(II)}^{PET}}\right) + \Delta\varphi^{PET-s} \qquad \text{(A9)}$$

where E^0 is the Os(III)/Os(II) standard redox potential *vs.* the Ag/AgCl/KCl 3 M reference electrode. We can approximate the activity of the Os complexes by their surface concentration in order to reformulate eqn (A9) in terms of the fraction of oxidized osmium sites: $f_O = \Gamma_{Os(III)}/\Gamma_{Os}$, where $\Gamma_{Os(III)}$ and Γ_{Os}

are the Os(III) and total osmium surface coverages, respectively. Thus, we have:

$$E = E^0 + \frac{RT}{F}\ln\left(\frac{f_O}{1-f_O}\right) + \Delta\varphi^{PET-s} \qquad (A10)$$

At this point we will assume that the PAD and the PET are the same and denote them hereafter as the end-group plane, EP.

The potential drop between the working and reference electrodes is given by:

$$E - E_{pzc} = \Delta\varphi^{M-EP} + \Delta\varphi^{EP-S} \qquad (A11)$$

where E_{pzc} is the potential of zero charge of the metal substrate. Combination of eqn (A10) and (A11) allows calculating the charge of the metal from the Gauss law as:

$$\sigma_M = \frac{\varepsilon_{film}\varepsilon_0}{d}\Delta\varphi^{M-EP} = \left[E^0 - E_{pzc} + \frac{RT}{F}\ln\left(\frac{f_O}{1-f_O}\right)\right]C_{film} \qquad (A12)$$

where d is the distance of the EP from the metal surface, ε_{film} is the relative dielectric constant of the organic layer and $C_{film} = \varepsilon_{film}\varepsilon_0/d$ is the capacitance of the organic layer (SAM or aryl diazonium monolayer) per unit area.

The total surface charge located at $z < d$ is compensated in the solution phase ($z > d$) by the diffuse ionic double layer. Using the Gouy–Chapman model (which is based on the Poisson–Boltzmann equation), we can write[31,40,48,49]

$$\Delta\varphi^{EP-S} = \frac{2RT}{F}\operatorname{asinh}\left[\frac{\sigma_{EP}+\sigma_M}{(8C_{salt}\varepsilon_s\varepsilon_0 RT)^{1/2}}\right] \qquad (A13)$$

where ε_s is the relative dielectric constant of the solution and the charge at the EP (σ_{EP}) has contributions from the redox and acid–base end-groups:

$$\sigma_{EP} = -F\Gamma_{HA/A}f + F\Gamma_{Os}[f_O(Z_{Os(III)} - Z_{Os(II)}) + Z_{Os(II)}] \qquad (A14)$$

where $\Gamma_{HA/A}$ is the total surface coverage of the weak acid groups. In order to use the system of equations (A9)–(A14) to fit the experimental data, we should assume that at the potential of the redox peak (*i.e.* for $E = E^{peak}$) the fraction of oxidized osmium species is one half (*i.e.* the redox peak potential corresponds to the apparent electrode potential of the Os couple), *i.e.* $f_O = 0.5$.[30,31,41] Since there is no explicit solution of E^{peak} as a function of C_{salt} or pH, we will provide parametric expressions in f.

For experiments performed at varying ionic strength and fixed pH, the following expressions can be obtained:

$$E^{peak}(f) = E^0 + \frac{2.303RT}{F}\left[pK_a - pH + \log\left(\frac{f}{1-f}\right)\right] \qquad (A15)$$

$$C_{salt}(f) = \frac{F^2}{8\varepsilon_s\varepsilon_0 RT}\left[\frac{-\Gamma_{HA/A}f + \Gamma_{Os}\frac{(Z_{Os(III)}+Z_{Os(II)})}{2} + \frac{(E^0-E_{pzc})C_{film}}{F}}{\sinh\left(\frac{2.303}{2}\left(pK_a - pH + \log\left(\frac{f}{1-f}\right)\right)\right)}\right]^2$$

$$\text{for } 0 < f < 1 \qquad (A16)$$

In the case of fixed C_{salt} and varying pH, we have:

$$E^{peak}(f) = E^0 + \frac{2RT}{F}\operatorname{asinh}\left[\frac{-\Gamma_{HA/A}f + \Gamma_{Os}\frac{(Z_{Os(III)}+Z_{Os(II)})}{2} + \frac{(E^0-E_{pzc})C_{film}}{F}}{\left(\frac{8C_{salt}\varepsilon_s\varepsilon_0 RT}{F^2}\right)^{1/2}}\right] \qquad (A17)$$

$$pH(f) = pK_a - \frac{2}{2.303}\operatorname{asinh}\left[\frac{-\Gamma_{HA/A}f + \Gamma_{Os}\frac{(Z_{Os(III)}+Z_{Os(II)})}{2} + \frac{C_{film}(E^0-E_{pzc})}{F}}{\left(\frac{8C_{salt}\varepsilon_s\varepsilon_0 RT}{F^2}\right)^{1/2}}\right] + \log\left(\frac{f}{1-f}\right) \quad \text{for } 0 < f < 1. \qquad (A18)$$

In both sets of eqn (A17) and (A18), there are five fitting parameters: pK_a, $(E^0 - E_{pzc})C_F$, E^0, $\Gamma_{HA/A}$ and Γ_{Os}. As explained in the text, for a given type of film the same fitting parameters were used to fit the data obtained under different pH and ionic strength conditions.

Acknowledgements

Financial support from ANCyPT, PICT 1146, PAE 2004 No. 22711, PAE-2006 No. 37063 and a CONICET PhD studentship are greatly appreciated.

References

1 A. Ulman, *An Introduction to Ultrathin Organic Films from Langmuir–Blodgett to Self-Assembly*, Academic Press, New York, 1991.
2 D. Dubois and R. G. Nuzzo, *Annu. Rev. Phys. Chem.*, 1992, **43**, 437.
3 J. C. Love, L. A. Estroff, J. K. Kriebel, R. G. Nuzzo and G. M. Whitesides, *Chem. Rev.*, 2005, **105**, 1103–1107.
4 J.-G. Lee, J. Lee and J. T. J. Yates, *J. Am. Chem. Soc.*, 2004, **126**, 440–441.
5 C. D. Bain, H. A. Biebuyck and G. M. Whitesides, *Langmuir*, 1989, **5**, 723.
6 G. M. Whitesides and P. E. Laibinis, *Langmuir*, 1990, **6**, 87–96.
7 K. R. Stewart, G. M. Whitesides, H. P. Godfried and I. F. Silvera, *Rev. Sci. Instrum.*, 1986, **57**, 1381.
8 S. R. Wasserman, H. Biebuck and G. M. Whitesides, *J. Mater. Res.*, 1989, **4**, 886.
9 K. L. Prime and G. M. Whitesides, *Science*, 1991, **252**, 1164.
10 S. E. Creager and J. Clarke, *Langmuir*, 1994, **10**, 3675–3683.
11 S. F. Scarlata and M. Rosenberg, *Biochemistry*, 1990, **29**, 10233.
12 A. Kumar, H. A. Biebuyck, N. L. Abbott and G. M. Whitesides, *J. Am. Chem. Soc.*, 1992, **114**, 9188.
13 J. M. Calvert, *J. Vac. Sci. Technol., B*, 1993, **11**, 2155.
14 C. E. D. Chidsey, *Science*, 1991, **251**, 919–922.
15 H. O. Finklea and D. D. Hanshew, *J. Am. Chem. Soc.*, 1992, **114**, 3173–3181.
16 G. K. Rowe and S. E. Creager, *J. Phys. Chem.*, 1994, **98**, 5500–5507.
17 S. E. Creager and K. Weber, *Langmuir*, 1993, **9**, 844–850.
18 G. K. Rowe and S. E. Creager, *Langmuir*, 1991, **7**, 2307–2312.
19 J. Petrovic, R. A. Clark, H. Yue, D. H. Waldeck and E. F. Bowden, *Langmuir*, 2005, **21**, 6308–6316.
20 M. Collinson, E. F. Bowden and M. J. Tarlov, *Langmuir*, 1992, **8**, 1247–1250.
21 M. A. Bryant and R. M. Crooks, *Langmuir*, 1993, **9**, 385.
22 J. Wang, L. M. Frostman and M. D. Ward, *J. Phys. Chem.*, 1992, **96**, 5224.
23 K. Shimazu, T. Teranishi, K. Sugihara and K. Uosaki, *Chem. Lett.*, 1998, 669.

24 L. Sun and R. M. Crooks, *Langmuir*, 1993, **9**, 1951.
25 F. Malem and D. Mandler, *Anal. Chem.*, 1993, **65**, 37.
26 L. Sun, B. Johnson, T. Wade and R. M. Crooks, *J. Phys. Chem.*, 1990, **94**, 8869–8871.
27 T. R. Lee, R. I. Carey, H. A. Biebuyck and G. M. Whitesides, *Langmuir*, 1994, **10**, 741–749.
28 C. D. Bain and G. M. Whitesides, *Langmuir*, 1989, **5**, 1370–1378.
29 V. Molinero and E. J. Calvo, *J. Electroanal. Chem.*, 1998, **445**, 17–25.
30 C. P. Smith and H. S. White, *Anal. Chem.*, 1992, **64**, 2398–2405.
31 C. P. Smith and H. S. White, *Langmuir*, 1993, **9**, 1–3.
32 M. E. Tagliazucchi, E. J. Calvo and I. Szleifer, *Langmuir*, 2008, **24**, 2869–2877.
33 M. W. J. Beulen, F. van Veggel and D. N. Reinhoudt, *Chem. Commun.*, 1999, 503–504.
34 A. M. Ricci, C. Rolli, S. Rothacher, L. Baraldo, C. Bonazzola, E. J. Calvo, N. Tognalli and A. Fainstein, *J. Solid State Electrochem.*, 2007, **11**, 1511–1520.
35 B. J. Barner, M. J. Green, E. I. Saez and R. M. Corn, *Anal. Chem.*, 1991, **63**, 55–60.
36 M. J. Green, B. J. Barner and R. M. Corn, *Rev. Sci. Instrum.*, 1991, **62**, 1426–1430.
37 B. L. Frey, R. M. Corn and S. C. Weibel, *Handbook of Vibrational Spectroscopy*, John Wiley & Sons, 2001.
38 N. Madhiri and H. O. Finklea, *Langmuir*, 2006, **22**, 10643–10651.
39 C. Danilowicz, E. Corton and F. Battaglini, *J. Electroanal. Chem.*, 1998, **445**, 89.
40 H. Ohshima and S. Ohki, *Biophys. J.*, 1985, **47**, 673–678.
41 J. Redepenning, B. R. Miller and S. Burnham, *Anal. Chem.*, 1994, **66**, 1560–1565.
42 D. W. Wang, R. J. Nap, I. Lagzi, B. Kowalczyk, S. B. Han, B. A. Grzybowski and I. Szleifer, *J. Am. Chem. Soc.*, 2011, **133**, 2192–2197.
43 W. R. Fawcett, M. Fedurco and Z. Kovčov, *Langmuir*, 1994, **10**, 2403–2408.
44 J. C. Love, L. A. Estroff, J. K. Kriebel, R. G. Nuzzo and G. M. Whitesides, *Chem. Rev.*, 2005, **105**, 1103–1169.
45 L. J. Wan, M. Terashima, H. Noda and M. Osawa, *J. Phys. Chem. B*, 2000, **104**, 3563–3569.
46 J. Wang and A. J. Bard, *J. Phys. Chem. B*, 2001, **105**, 5217–5222.
47 K. Hu, Z. Chai, J. K. Whitesell and A. J. Bard, *Langmuir*, 1999, **15**, 3343–3347.
48 A. J. Bard and L. R. Faulkner, *Electrochemical Methods*, John Wiley and Sons, New York, 2nd edn, 2001.
49 C. P. Smith and H. S. White, *Anal. Chem.*, 1993, **65**, 3343–3353.